Limits on High Specific Impulse Ion Thruster Operation

Paul J Wilbur*
Department of Mechanical Engineering
Colorado State University, Fort Collins, CO 80523-1374

An experimental study of high specific impulse (high net accelerating voltage) optics operating on argon, krypton or xenon is presented. Trends in backstreaming voltages and perveance-limited beamlet currents are investigated and correlations are made with the appropriate theories. Effects of changes in grid parameters are examined. The concept of a single beamlet thruster is discussed.

Introduction

As interest in increasingly ambitious deep space missions develops thruster specific impulses selected to optimize delivered payload fractions increase. These specific impulse increases must be coupled with increases in thruster power to realize design thrust levels. In ion thrusters where the ion production, acceleration and neutralization processes are generally separable, the process of ion acceleration to high specific impulse levels can be addressed first and a discharge (ion production) chamber can then designed to match the demands of the ion optics. For the high specific impulse thruster built and tested in the mid 1960's the result was a 1.5-m-diameter thruster with two, match-drilled, multiaperture acceleration grids separated by several millimeters.[1] The thruster was operated on mercury at nominal net accelerating voltage and ion beam current conditions near 5 kV and 16 A, respectively. These conditions yielded specific impulse and beam power conditions near 8 ks and 80 kW, respectively.

This paper is focused on the same, simple two-grid ion acceleration concept used in the 1.5-m thruster but it reflects recent technological advances and addresses the relative benefits of xenon, krypton and argon propellants. The range of specific impulses that can be realized using these propellants is determined by the definition of specific impulse and conservation of ion energy during the acceleration process and is given by

$$I_{sp} = \frac{\eta_u \eta_d}{g_o}\sqrt{\frac{2\,e\,V_N}{m}} \quad . \qquad (1)$$

In this equation η_u and η_d are the propellant utilization and beam divergence efficiencies, respectively, g_o the Earth sea level gravitational acceleration, e the electronic charge, m the ion mass and V_N the net acceleration voltage. Divergence efficiencies are typically near unity, so this value was assumed and the values shown in Fig. 1 were computed for the three propellants. The utilization efficiencies indicated for each propellant are those that yield discharge chamber operation at the performance curve knee as determined by Brophy using his discharge chamber model.[2] The Eq. 1 results in Fig. 1 show the net accelerating voltage required for operation at a prescribed specific impulse can be reduced by using a lower propellant ion mass. Such reductions not only mitigate electrical breakdown/insulation problems but they enable lower electron backstreaming voltages that in turn yield lower accel grid sputtering rates and hence longer lifetimes.

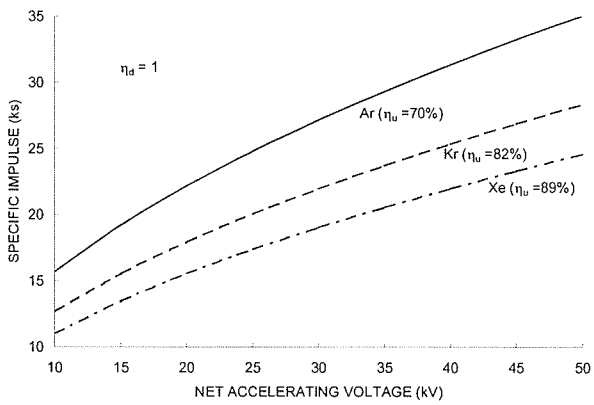

Fig. 1 Theoretical Effect of Net Accelerating Voltage and Ion Mass on Specific Impulse

Apparatus and Procedures

In order to evaluate further the suitability of Ar, Kr and Xe at high specific impulse, high beam power ion thruster operating conditions and to select preferred ion optics system dimensions, gridlet tests[3] were conducted using the discharge chamber/grid assembly shown schematically in Fig. 2. It is a 9.2-cm inside diameter chamber with mild steel cylindrical sidewall and upstream plates and a 304 stainless steel downstream grid mounting plate. The upstream Alnico V

* Professor, AIAA Senior Member

magnet and cone couple with the samarium cobalt ring magnet and ferromagnetic wall circuit to produce a magnetic field that facilitates ion flow toward a relatively weak magnetic field region at the screen grid aperture. Ionizing electrons are drawn from a heated cathode filament that is usually arranged as two 3-cm radius semicircles that are suspended from mounting rods so they are centered in the ring magnet cusp. In this magnetic field/filament configuration it is argued that emitted electrons ionized within a large region of the chamber and produce a relatively uniform (albeit unmeasured) density plasma at the screen aperture. For some tests, the filament was arranged so it protruded toward the screen aperture in a configuration expected to produce plasma density profiles that were peaked on the chamber centerline. A single pair of screen and accel apertures machined in Poco graphite plates mounted, respectively, on the downstream stainless steel plate and on an insulating structure served as the ion optics assembly.

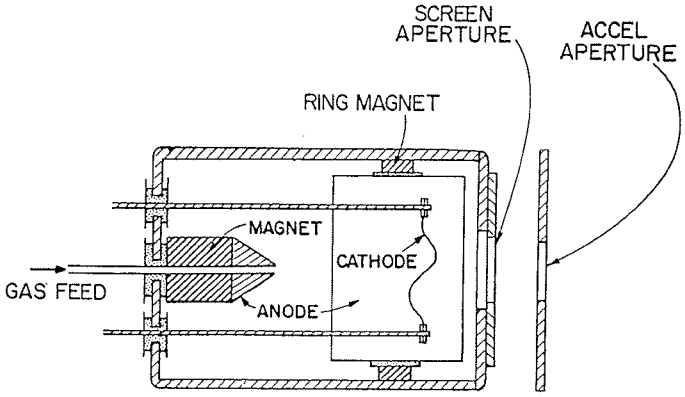

Fig. 2 Schematic of Ion Source and Optics Set

Tests were conducted in a 42-cm diameter vacuum chamber that was diffusion-pumped to $< 7\text{x}10^{-7}$ Torr prior to testing. A tungsten filament neutralizer positioned at the beamlet edge and biased –40 V relative to tank ground and heater to the point where it emitted an electron current ~4 mA greater than the beamlet current was used for beam neutralization. After establishment of a stable propellant flow and plasma discharge condition at a discharge voltage that could not be measured but was estimated to be 35 V the beamlet current was set at a value about midway between the crossover and perveance limits[3] associated with a selected net accelerating voltage. The potential on the accelerator grid was set significantly below the value where electron backstreaming was expected. Data like those shown in Fig. 3 were collected digitally as the voltage on the accelerator grid was increased. The voltage at which electron backstreaming occurred was determined by drawing straight lines through the two linear data segments that are apparent in Fig. 3. The intersection of these lines is designated the backstreaming limit at the selected beamlet current (13.5 mA for Fig. 3). Oscillations in beamlet current, which are apparent in the data of Figs. 3 were observed in most data sets. The symbols in the legend of Fig. 3 are the usual ones used to define a grid geometry[3]. They are: ℓ_g, the grid separation; d_s, the screen aperture diameter; d_a, the accel aperture diameter; t_s, the screen grid thickness; and t_a, the accel grid thickness.

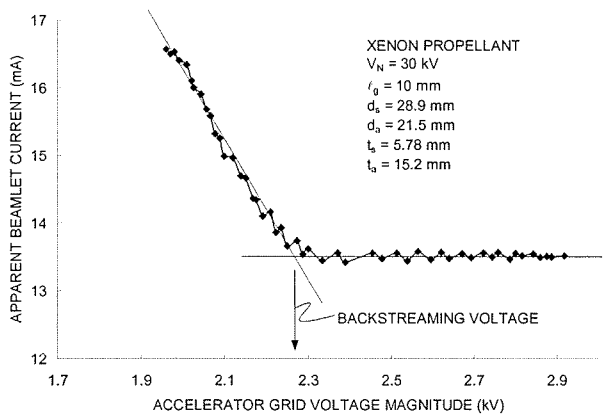

Fig. 3 Typical Electron Backstreaming Data Set

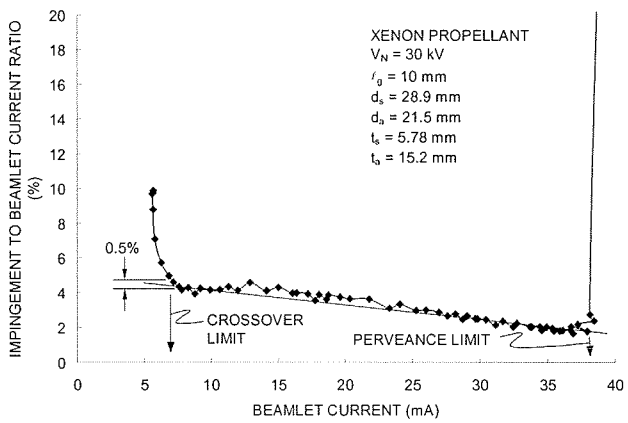

Fig. 4 Typical Impingement Current Data Set

The range of beamlet currents over which grids with a prescribed geometry can be operated without direct ion impingement on the accel grid was also investigated. Measurements required to determine this range were made by first biasing the accel grid ~250 V more negative than the backstreaming voltage, sweeping the beam current and measuring the beam and impingement current. Figure 4 is a typical plot generated from data recorded digitally starting at a low beamlet current and increasing cathode filament current gradually to induce a corresponding increase in beamlet current to the point where impingement current rose abruptly. Crossover and perveance limits on direct impingement of beam ions were determined from this plot of impingement-to-beamlet current ratio vs. beamlet current by drawing a straight line through the linear data regions near the limits. The beamlet current at crossover (i.e. the crossover limit) was determined by finding

the impingement-to-beamlet current (i-to-b) ratio at the intersection of this line and the one joining data points, adding 0.5% to it, and picking off the beamlet current corresponding to this value of the i-to-b ratio. The perveance limit was generally determined by inspection, as the i-to-b ratio rose abruptly and it was unnecessary to follow the crossover procedure to establish the limit accurately.

It is noted that the flow into the source is constant and the neutral loss rate through the grids must decrease as beamlet current is increased. It is believed that this results in a decrease in charge exchange ion production which in turn causes the decrease in the i-to-b ratio over the baseline data region in Fig. 4. It is noted further that propellant flow rates were established using preliminary versions of data like those shown in Fig. 4. This was done by setting a flow that yielded an i-to-b ratio near 2% at the perveance limit. Ratios significantly below this value could cause the chamber discharge to extinguish before the perveance limit was reached.

Results

Initial tests were conducted on a reference grid set with the same proportions as a grid set in common usage (the NSTAR set). Dimensions were scaled up from those for this grid set so the commonly used intragrid electric field of 2 kV/mm would exist at the nominal net accelerating voltage of 20 kV. Plans called for testing below this value to 10 kV and then as high above it as electrical breakdown and power supply limitations would allow. It turned out that a power-supply-imposed limit on the accel grid voltage that could be applied (-3 kV) constrained operation to a maximum net accelerating voltage of 30 kV. As a consequence the electric field range investigated was 1 to 3 kV/mm.

The backstreaming voltage and perveance limited beamlet current data measured for the reference grid set operating on argon, krypton and xenon are shown in Fig. 5. The backstreaming voltage data in Fig. 5a for each propellant are all described with reasonable accuracy by the following approximate equation for backstreaming voltage developed by Kaufman[4] at a backstreaming margin (V_{margin}) of zero.

$$|V_a| = \frac{k V_N}{\frac{\ell_e}{d_a}\exp\left[\frac{t_a}{d_a}\right] - k} + V_{margin} \qquad (2)$$

where the constant k is about 0.17, and ℓ_e is given by

$$\ell_e = \sqrt{(\ell_g + t_s)^2 + \frac{d_s^2}{4}} \quad . \qquad (3)$$

The nearly horizontal lines in Fig. 5a are lines of constant net accelerating voltage and results would be independent of propellant if those lines were exactly horizontal. Extrapolation of the results of Fig. 5a suggests the backstreaming voltage there would have been near –3 kV at a 30 kV net accelerating voltage. Because there would have been no margin against backstreaming at this net accelerating voltage with the available power supply, reliable data could not collected with the reference grids. Perveance limited beamlet current data shown in Fig. 5b show effects of total accelerating voltage ($V_T = V_N + |V_a|$) and propellant atom mass (m_p) that are generally consistent with the Child-Langmuir law modified to

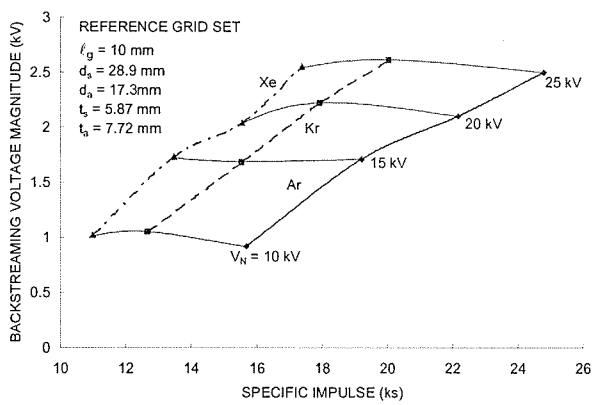

Fig. 5a Reference Grid Set Backstreaming Map

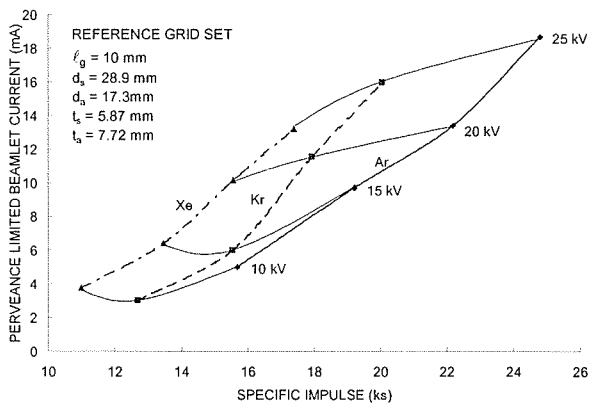

Fig. 5b Reference Grid Set Perveance Map

accommodate ion optics geometries using the effective acceleration length (ℓ_e again defined by Eq. 3). This law which given below it gives the current that can be extracted from a single aperture set in terms of a the constant permittivity of space (ε_o) is:

$$J_b = \frac{p e_o}{9}\sqrt{\frac{2e}{m_p}}\,V_T^{3/2}\,\frac{d_s^2}{\ell_e^2} \quad . \qquad (4)$$

The consistency of the data in Fig.5b are reflected in the fact that the ratio of net (and total) accelerating voltages is 25 kV/ 10 kV = 2.5 and the ratio of the currents at these voltages for each propellant is about $2.5^{3/2} \approx 4$. In the case of the least massive propellant atom (Ar) the maximum current that can be extracted in a beamlet through the single hole pair is over 18 mA. Crossover beamlet current limits, which are expected to be of lesser concern in high specific impulse thrusters, are not given here by they were generally about 40% of the Child-Langmuir limits for the reference grids.

The data of Fig 5a indicate that acceleration grid voltage magnitudes increase well into the kV range and it would be desirable to reduce these voltages to control accel grid sputter erosion rates and hence increase grid lifetimes. It would also be desirable to increase the perveance limit on the beamlet current that can be extracted to increase the thrust per beamlet for a thruster. Some work was done to determine if the grid geometry could be altered to induce these beneficial effects. Figures 6a and b show the effects of some of the grid parameter changes that were investigated to reduce backstreaming voltages and increase perveance-limited beamlet currents. To facilitate a ready evaluation of trends data are presented for argon only, but the trends shown are consistent with the results obtained with the other propellants. Equation (3) indicates the backstreaming voltage can be reduced by increasing the grid spacing (ℓ_g) and comparison of the solid and centerline curves in Fig. 6a shows a 50% increase in ℓ_g did induce a reduction of some hundreds of volts. On the other hand, comparison of corresponding curves in Fig. 6b shows the spacing increase induced a several mA beamlet current reduction at each corresponding net accelerating voltage. It is noted that this would also be the case at 30 kV in a situation where there was not a limit on the accel-grid-power-supply output voltage. One way the beamlet current could be increased would be to increase the accel grid hole diameter (d_a) and the effect of increasing it 24% above the reference grid value can be seen by comparing the solid and dashed curves in Figs. 6a and 6b. Figure 6b shows that this change does enable beneficial (few-mA) increases in beamlet current, but Fig. 6a shows it would necessitate undesirable kV-level increases in the magnitude of the accel grid voltage.

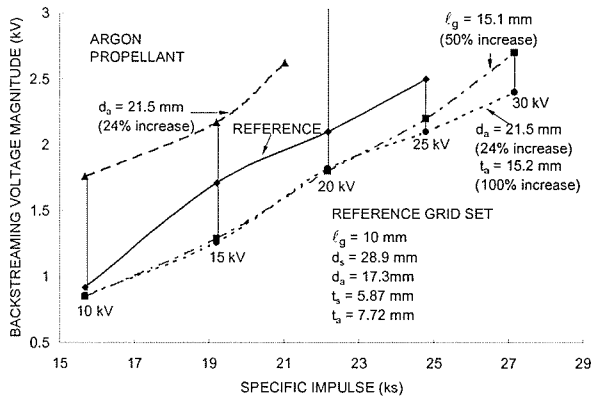

Fig. 6a Effect of Grid Changes on Backstreaming

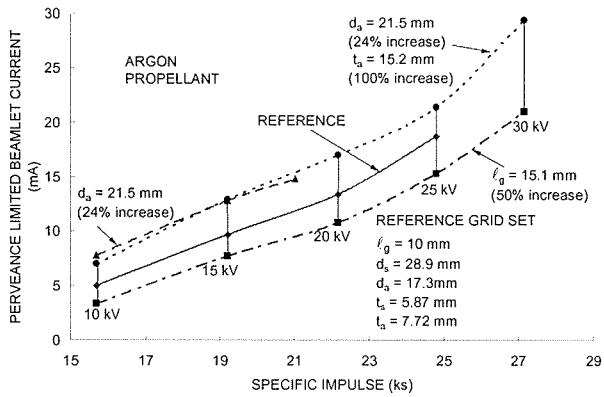

Fig. 6b Effect of Grid Changes on Perveance Limit

A more attractive change in grid geometry involves a concurrent increase in both the diameter and thickness of the accel grid. The beneficial effect of these changes relative to the reference grid can be seen by comparing the solid and dotted curves in Figs. 6a and 6b for the case where accel hole diameter was increased by 24% and accel grid thickness (t_a) was doubled. This comparison shows concurrent kV-level reductions in backstreaming voltage magnitudes and several-mA-level increases in beamlet current. From a physical point of view, these accel grid changes enable improvement because the increase in accel grid thickness reduces the backstreaming voltage (Eq. 3) but does not significantly reduce beamlet currents, which increase with accel hole diameter. The backstreaming voltages and perveance-limited beamlet currents measured using all three propellants on this selected grid set are given in Figs. 7a and 7b. They all show consistent reductions in backstreaming voltage magnitude and increases in current compared to the reference grid set (Fig. 5).

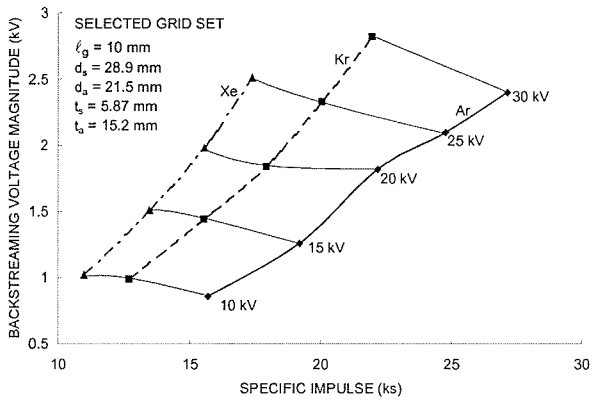

Fig. 7a Selected Grid Set Backstreaming Map

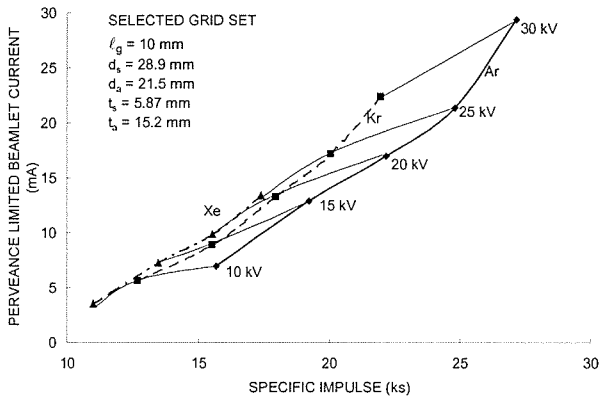

Fig. 7b Selected Grid Set Perveance Limit Map

With an admittedly not optimized, but suitable ion optics (grid) system selected for high specific impulse operation, it is appropriate to consider the interface between the discharge plasma and the grids. Discharge plasma measurements have not yet been made in the discharge chamber used in this study, but it is argued that the electron-emitting filament was arranged so it would produce a relatively uniform discharge plasma at the screen hole for all of the test results reported in preceding figures. This was accomplished by mounting the filament shown schematically in Fig. 2 so it extended from its mounting posts in two semicircular arcs with a radius just a few millimeters less than the radius of the ring-magnet anode and was positioned axially in the well of the magnetic field cusp at that anode. Thus, the filament was positioned radially as suggested by the centerline-view sketches associated with the solid curves in Figs. 8a and 8b. In a traditional ion thruster with many hole pairs in the grids, the holes are small and the discharge plasma properties, which could vary slowly between screen grid holes over the full beam diameter, should be quite uniform across each screen hole. For the small ion source of Fig. 2 coupled with the large diameter screen hole used in this study, however, one might expect substantial plasma density variations could be induced across the screen hole sheath. In the course this study intentional changes were introduced in the configuration of the cathode filament that, it is argued, induced axisymmetric plasma density variations across the sheath. First two filaments of the same length as the original ones were looped downstream so the centerline view of them would be as suggested by the sketch associated with the dashed curves in Fig. 8. Next the filament support posts were moved close to the discharge chamber centerline so a filament of the same length could be confined to a region very close to the centerline as suggested by the sketch associated with the centerline curves. It is argued qualitatively that this sequence of changes in filament position should result in progressively greater fractions of electron emission and ion production near the centerline thereby producing greater plasma densities there.

The plots of Fig. 8 were obtained using xenon propellant. Those in Fig. 8a indicate the two changes from the initial (uniform plasma density) state caused the backstreaming voltages to first increase above and then to decrease below the uniform state curve represented by the solid curve. These data suggest that the lowest backstreaming voltage is realized when the plasma density profile at the sheath is most peaked. Figure 8b shows the perveance-limited beamlet currents realized with both of the peaked profiles are 2 or 3 times those for the uniformly distributed plasma (solid curve). The corresponding comparison of beamlet powers (the product of beamlet current and net accelerating voltage at each operating

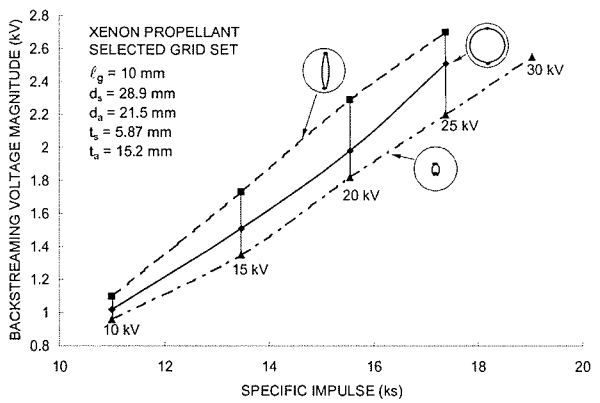

Fig. 8a Effects of Plasma Uniformity on Backstreaming

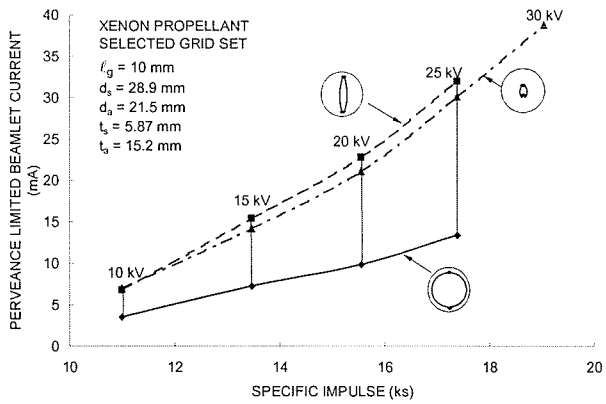

Fig. 8b Effects of Plasma Uniformity on Perveance Limits

condition) are plotted in Fig. 8c. This figure suggests the peaked plasma density profiles enable beamlet powers that are about double those for the uniform density case. The beamlet current range is defined as the difference between the beamlet currents at the perveance and crossover limits and the data of Fig. 8d indicates this range can be increased by about a factor of three by changing from a uniform to a peaked plasma density profile across the screen aperture sheath. This implies that operation with a peaked density profile would also be attractive for missions on which a wide throttling range was required.

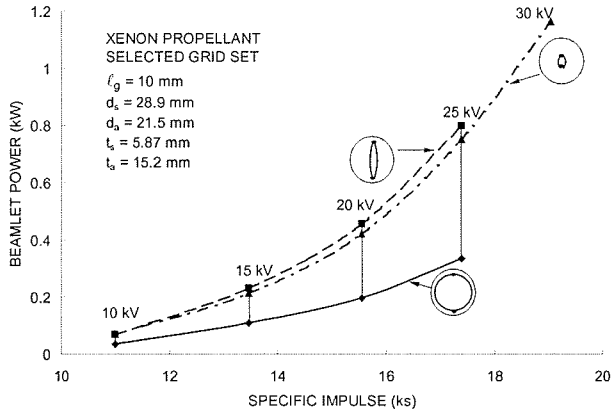

Fig. 8c Effect of Plasma Uniformity on Beamlet Power

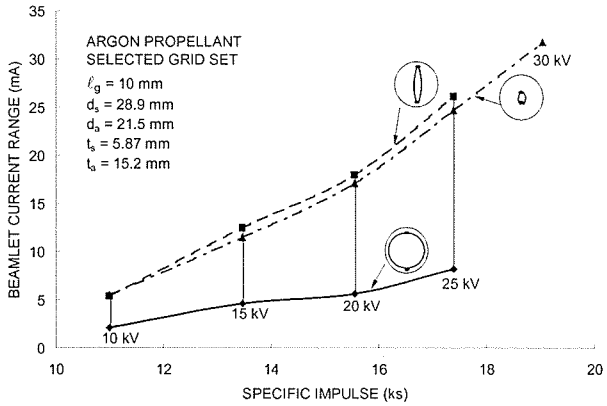

Fig. 8d Effect of Plasma Uniformity on Current Range

It is of interest to consider the usefulness of the Child-Langmuir law (Eqs. 3 and 4) as a normalizing factor for the perveance and crossover limits at the high specific impulses where these experiments have been conducted. Using Eq. 2 to compute the acceleration grid voltage required to prevent backstreaming and adding it to the associated net accelerating voltage yields a total accelerating voltage that can be used in Eq. 4 to compute a theoretical perveance limit. Dividing this into corresponding measured beamlet currents yields normalized beamlet currents like those plotted against net accelerating voltage in Fig. 9 for the various propellants and the case of the selected grid with a uniform plasma density at the sheath. If the Child-Langmuir theoretical perveance limit modeled the effect of accelerating voltage perfectly for both the perveance and crossover limits, the lines in Fig. 9 would all be horizontal and if it modeled the effect of mass perfectly, they would be coincident. They are neither, but their departure from this ideal, which is probably due primarily to experimental and data analysis errors, is considered acceptable for a rough model. The numbers after each propellant designation in Fig. 9 are the means of the 4 or 5 percentages for each propellant/limit case. Taken together the results of Fig. 9 suggest the perveance and crossover limits for grid sets such as these could be estimated at 45% and 20%, respectively, of the corresponding Child-Langmuir theoretical perveance limit.

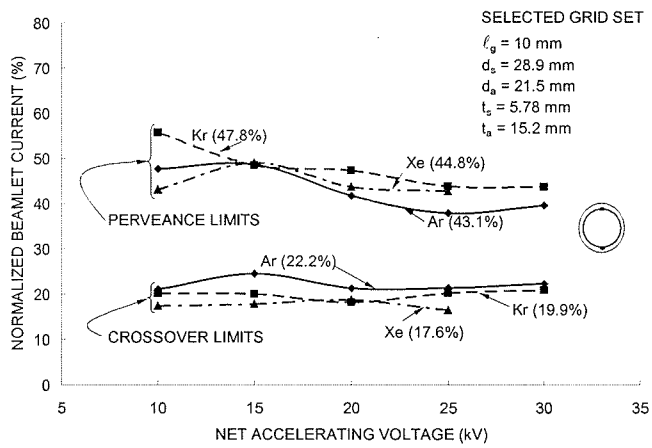

Fig. 9 Effect of Net Accelerating Voltage on Langmuir Law Normalization

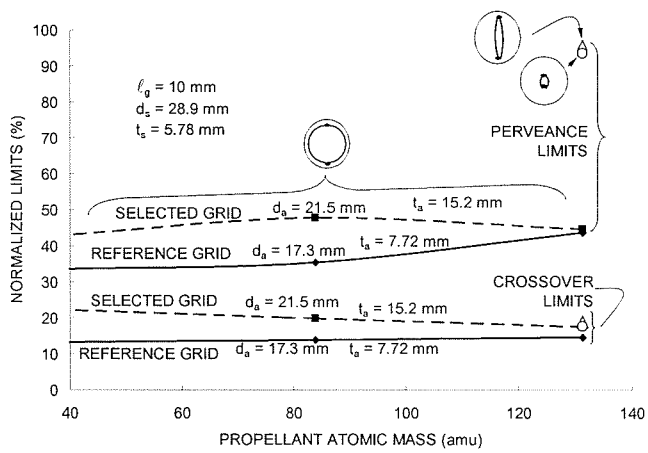

Fig. 10 Effect of Grid and Chamber Plasma Changes on Langmuir Law Normalization

When measured perveance and crossover limits are normalized and averaged over net accelerating voltage, data like those shown in Fig. 10 are obtained. This figure compares normalized limits for the selected and standard grid sets as a function of propellant mass and the near-horizontal lines imply that the effects of propellant mass are modeled quite well. It is reasonable for both the perveance and crossover limits on the selected grid set to be greater than those for the reference set because the selected set has a larger accel aperture diameter that would accommodate greater beamlet divergence and therefore greater currents at both limits. The limits for the selected grid sets with peaked plasma density profiles at the screen grid, designated by the open data symbols at 131 amu in Fig. 10 are of particular interest. They show that for both of the peaked plasma density profile cases, the normalized crossover and perveance limits are at 20% and almost 100%, respectively, of the corresponding Child-Langmuir theoretical perveance limit.

Discussion

As thruster specific impulses increase, grid separations, aperture diameters, and consequently the current and power associated with each beamlet can all also increase. The point is eventually reached kilowatt power levels are being extracted through individual aperture pairs and the question of whether it might be advantageous to operate many separate discharge chambers from which single beamlets are extracted rather than solitary discharge chambers with multiaperture grids arises. Results from this study suggest the beamlet current and power could be about doubled through plasma density profiling across the screen grid of a single aperture thruster and further research may point the way to even further increases. This would also eliminate the need for the difficult-to-achieve flat beam profiles required in large, mutliaperture thrusters. Additional advantages of the single beamlet thruster might be the ability to operate each beamlet near the perveance limit, the ability to throttle over a wider range, the elimination of problems associated with erosion into adjacent grid apertures, and a high level of redundancy. Disadvantages could include increased complexity with many additional components including cathodes and those for flow and power electronics needs. Discharge chamber beam ion energy costs would also expected to be higher for the single beamlet thruster but at high net accelerating voltages electrical efficiencies would still be expected to be near unity.

In order to estimate the performance capability of a single aperture thruster over a range of specific impulses with the inert gas propellants studied, operation at the Child-Langmuir law perveance limit (i.e. the selected aperture set with a tailored plasma profile) will be assumed. The effects of propellant and specific impulse on beamlet power for this case are given in Fig. 11. This figure shows the benefit of using less massive propellant to realize lower net accelerating voltages and powers at a prescribed specific impulse. It is noted, however, that the lines of constant net accelerating voltage are also essentially lines of constant thrust (1.3 mN @10 kV, 2.9 mN @ 20 kV, 5.2 mN @ 25 kV, and 11.8 mN @ 30 kV). Hence operation with lighter propellant atoms also yields lower thrust. It is noteworthy that Fig. 11 shows a single beamlet power over 2 kW at 27 ks specific impulse with argon.

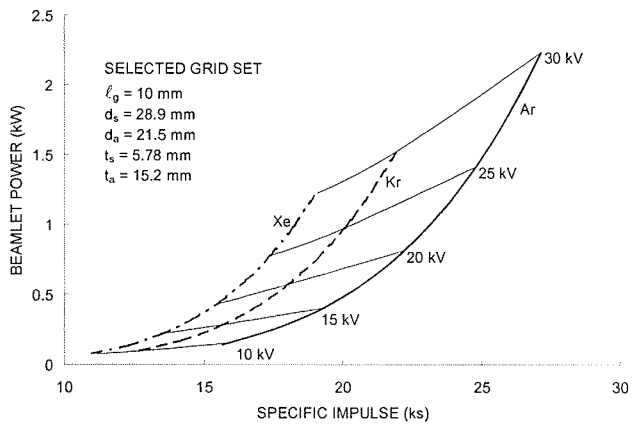

Fig. 11 Theoretical Peak Power Capability Map for Selected Grid with Tailored Discharge Plasma Profile

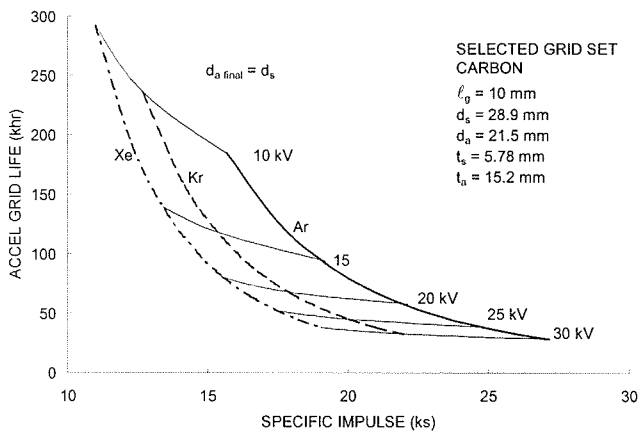

Fig. 12 Theoretical Accel Grid Life Map for Selected Grid with Tailored Dischaarge Plasma Profile

It is well to point out again here that data show a single beamlet thruster with a peaked discharge plasma density profile can operate at the Child-Langmuir perveance limit. For multiaperture grids where such profiling is not possible the data suggest the grids pertaining to Fig. 11 would have a maximum beamlet current and hence beamlet power about 45% of the Child-Langmuir limit limit values assumed for the figure. Additional research on perveance limits indicates the adjacent

hole effect would reduce the pervance limit by about an additional 10%.[5] Hence the data of Fig. 11 could be used for multiaperture applications of the grid dimensions cited if the beamlets powers that were 40% of those cited were used. Crossover limits of Fig. 10 suggest are at ~ 20% of Child-Langmuir limits do not seem to be affected significantly by the adjacent-hole effect unless the screen grid is very thin.

The simple model developed in the appendix was applied to evaluate the effects of specific impulse and propellant on the charge-exchange-ion, sputter-erosion-dependent lifetime of a carbon accel grid for the case of the selected grid and a peaked discharge plasma profile. In applying this model, it was assumed that 0.4% of the beam ions that pass through the grid charge exchange and that all of the resulting charge exchange ions sputter the barrel of the accel grid with the kinetic energy they would acquire passing through the full ground-to-accel potential difference. The effects of redeposition and resputtering and of increases in the accel grid voltage required to prevent backstreaming with a 100-V margin as the accel aperture diameter increases are included. Sputter yields at these energies are determined using the model of Yamamura and Tawara.[6] Because there are no adjacent holes in the single beamlet thruster erosion of accel grid material could probably continue through the full duration of even the most ambitious missions currently under consideration. For the purposes of this study, however, it was assumed that end of accel grid life occurred when the accel aperture diameter sputter eroded to that of the screen grid aperture. It is noted, however, that enlargement of the accel grid barrel on the NSTAR grids essentially stopped when its diameter had increased by about 24%.[7] The same behavior might also be expected in this case.

The accel aperture barrel sputter-erosion-limited lifetime results for the selected grid operating at the same perveance limited condition as for Fig 11 and with the assumptions mentioned are shown in Fig. 12. They reveal the clear benefit of operation on a light propellant and the long lifetimes that can be expected in general. Argon gives the longest lilfetimes both because the lowest net accelerating voltages are required for operation at a prescribed specific impulse and because sputter yields become progressively lower as atomic masses of these inert gases decrease. It is also worth noting that the marginal increases in sputter yields with energy become relatively smaller in the kilovolt range as the peak in the yield vs. energy plot is approached.

Conclusions

When a two-grid ions optics system is operated at the high voltages required from high specific impulse operation, expected changes in backstreaming voltage and perveance-limited beamlet current are observed with changes in grid separation, accel hole diameter and accel grid thickness. In comparison to a reference grid set scaled up from NSTAR dimensions a set with an accel grid that is proportionally thicker with a larger aperture diameter operates at lower backstreaming voltages and greater perveance-limited beamlet currents. Simple models of these voltage and current limits are adequate to describe the generally observed experimental behavior. The reference grid exhibits perveance and crossover limited currents extracted via a single beamlet that are about 40% and 15%, respectively, of theoretical Child-Langmuir perveanace limits. When the larger accel aperture is used these increase to about 45% and 20%, respectively, of the theoretical perveance limit. If the discharge plasma is tailored so it is more dense on the centerline of the screen aperture sheath, the crossover limit remains at 20% but the perveance-limited current can be increased to almost 100% of the theoretical limit with this same grid set. Beamlet currents and powers increase with specific impulse and it may be advantageous to use single rather than multibeamlet thrusters in some high specific impulse applications. By using less massive beam ions (e.g. Ar rather than Kr) beamlet powers and accel grid lifetimes will both be greater at a given specific impulse

References

1. Nakanishi, S., and E.V. Pawlik, "Experimental Investigation of a 1.5-m-diam Kaufman Thruster," J. Spacecraft, V. 5, No. 7, July 1968, pp. 801-807.

2. Brophy, J.R., "Ion Thruster Performance Model," Ph.D. Dissertation, Colorado State University, (also NASA CR-174810), Dec. 1984, p91.

3. Wilbur, P.J., J. Miller, C. Farnell, and V.K. Rawlin, "A Study of High Specific Impulse Ion Thruster Optics," International Electric Propulsion Conference Paper IEPC-01-098, Pasadena, CA, Oct. 15-19, 2001.

4. Kaufman, H.R., "Technology of Electron-Bombardment Ion Thrusters", *Advances in Electronics and Electron Physics*, V. 36, pp. 301-303, Academic Press, San Francisco, 1974

5. Williams, J.D., Colorado State University Monthly Letter to John Foster, November 26, 2003.

6. Yamamura, Y and H. Tawara, "Energy Dependence of Ion-Induced Sputter Yields from Monatomic Solids at Normal Incidence," Atomic Data and Nuclear Data Tables, v. 62, No. 2, March 1996, pp 149-253

7. Sengupta, A, JR Brophy, KD Goodfellow, "Status of the Extended Life Test of the Deep Space 1 Flight Space Ion Engine after 30,352 hours of Operation, Joint Propulsion Conference Paper AIAA-2003-4558, July 20-23, 2004.

8. Holman, J.P., *Heat Transfer*, McGraw Hill, 1981, pp. 319-324.

Appendix
Accel Grid Life Model Development

The number of beam ions ΔN_+ that will be extracted from an ion thruster that processes ΔM_p kg of propellant at a propellant utilization efficiency η_u when each propellant ion has a mass m_p is given by

$$\Delta N_+ = \frac{\Delta M_p \, \eta_u}{m_p} . \qquad \text{(A1)}$$

The number of charge exchange ions ΔN_{ib} that will impinge on the barrels of accel grid holes as a result of interactions between neutrals and the beam ions that pass through grids is given by

$$\Delta N_{ib} = \Delta N_+ \, f_i \qquad \text{(A2)}$$

where f_i is the impingement-to-beam current ratio and it is assumed conservatively that all ions that impinge on the accel grid strike in the barrel region. The mass loss from the accel grid barrel as a result of this impingement is given by

$$\Delta M_{ab} = \Delta N_{ib} \, Y \, m_a \, r \qquad \text{(A3)}$$

where m_a is the mass of an accel grid atom, r is the fraction of sputtered atoms that will actually be lost from the barrel region of the accel aperture (i.e. those that will not have to be re-sputtered), and Y is the sputtering yield. The mass loss from the accel grid aperture can also be expressed in terms of an incremental change in accel grid hole diameter Δd_a from a value d_{ai} at the start of the incremental erosion period to a final one d_{ai}-Δd_a by the equation

$$\Delta M_{ab} = \frac{\pi}{4} t_a \, \rho_a \, (2 \, d_{ai} \, \Delta d_a - \Delta d_a^2) \qquad \text{(A4)}$$

where t_a is the accel grid thickness and ρ_a is the mass density of the accel grid material.

The time (ΔT) required to process a propellant mass ΔM_p is related to the ion beam current (J_B) by the equation

$$\Delta T = \frac{\Delta M_p \, e \eta_u}{J_B \, m_p} \qquad \text{(A5)}$$

where e is the electron charge. Combining Eqs. (A1) through (A5) to eliminate ΔM_p, ΔN_+, ΔN_{ib}, and ΔM_{ab} one obtains

$$\Delta T = \frac{\pi \, t_a \, \rho_a \, e \, (2 \, d_{ai} \, \Delta d_a - \Delta d_a^2)}{4 \, Y \, r \, f_i \, m_a \, J_B} \qquad \text{(A6).}$$

Equation (A6) is now solved for ΔT at a specified net accelerating voltage (V_N) for each incremental reduction in d_a, computing at each accel hole diameter 1) the accel voltage required to prevent backstreaming ($|V_a|$ from Eqs. 2 and 3), 2) the total accelerating voltage (sum of $|V_a|$ and V_N), 3) the beam current at the perveance limit (Eq. 4), 4) the sputter yield at the mean impact energy of the charge exchange ions (assumed equal to $|V_a|$) and 5) the sputtered ion loss fraction (r). The total time for erosion to a final accel hole diameter $d_{a\,final}$ is then the sum of the values of ΔT.

The grid atom fractional loss factor r is determined by the apparent size of the cylindrical walls of the accel aperture barrel region. Since the atoms will either escape or hit the barrel, this barrel view factor F_v is related to r by the equation

$$r = 1 - F_v \qquad \text{(A7)}$$

where F_v has been obtained by curve fitting analogous radiation heat transfer view factor data[8] to obtain the equation:

$$F_v = 0.0154 \, (2 \, t_a/d_a)^3 - 0.139 \, (2 \, t_a/d_a)^2 + 0.507 \, (2 \, t_a/d_a) - 0.0002 . \qquad \text{(A8)}$$

As barrel erosion occurs in the accel hole, the value of r changes and Eqs. (A7) and (A8) are used to compute the variation in r with these increases in d_a.